

Direct electromagnetic source tomographic imaging neurotechnology (DESTIN).

Giorgio Bonmassar

*A. A. Martinos Center, Harvard Medical School, Massachusetts General Hospital,
Charlestown, MA, USA*

Correspondence: G Bonmassar, A. A. Martinos Center, Harvard Medical School,
Massachusetts General Hospital, Building 149 13th Street, Charlestown, MA 02129,
USA. E-mail: giorgio.bonmassar@mgh.harvard.edu,
phone +1 617 726 0962, fax +1 617 726 74222.

Abstract. One of the technique that have the greatest chance for being both high impact and disruptive is electroencephalography (EEG) because of the low cost of the device, installation, operation and ease of use. EEG is universally used in neuroscience research. Despite its great success and demonstrated potential for brain imaging, significant limitations exist with EEG, most important of which is the accuracy of the localization of the brain sources from the recorded EEG due to the ill-posed nature of the localization procedures which lead multiple solutions. This is solved by fMRI, or blood oxygen level dependent, is a well-established method for cognitive and clinical neuroscience as hemodynamic data are the epiphenomena of underlying neuronal activity. Brain mapping is one of the major endeavors that has been recently undertaken in neuroscience using fMRI to noninvasively localize the various brain functions. However, fMRI still has time resolution limitations and subjects can only be studied in the confines of an MRI scanner.

Direct Electromagnetic Source Tomographic Imaging Neurotechnology (DESTIN), may allow us to study subjects outside a scanner room and with ms second resolution needed to study neuronal activity. DESTIN is uniquely based on an entirely new physical principle which does not rely on EEG signals alone for electrical source localization rather time of flight localization as it is similarly done in PET. Time-of-flight measurements are used for distance measurements where a source sends out a short energy pulse (electromagnetic, optical, sound, etc.) and detector measures the time until the reflected pulse is sensed. In most cases the temporal accuracy must be very high for instance 1 ns resolution for a spatial accuracy of 15 cm in the case of a light pulse travelling in air. By circumnavigating the inverse problem with the new concept of time of flight instead, this method will enable researchers to study functional activity with millimeter spatial resolution and unprecedented high temporal resolution. The theory predicts that a 10 Hz brain alpha wave travels in white matter at a speed of 44,721 m/s, or almost 7,000 \times slower than the speed of light. Thus, DESTIN will have to be sensitive enough to detect down to a 1mm spatial resolution or phase delays of $\tau_p=22.4$ ns. However, Finite Element Method simulations on a human model illustrate the added complication of space-variant phase distribution, which is dependent on the position of the source. Finally, a MATLAB-based localization illustrates how the source tomography can be implemented. In conclusion, this novel method may become the next generation brain imaging technology, providing a direct measure of neuronal

activity with the exquisite millisecond resolution of EEG and millimeter spatial resolution in brain space at low cost and high degree of portability for real world measurements.

Keywords: inverse solution, EEG, Bioelectromagnetism, tomography, time of flight.

1. Introduction.

The demand for non-invasive human brain imaging has grown rapidly over the past decade as researchers and clinicians seek to advance understanding of the human brain. One of the techniques that has the greatest chance for being both high impact and disruptive is electroencephalography (EEG) as measured by Direct Electromagnetic Source Tomographic Imaging Neurotechnology (DESTIN). The proposed novel EEG is potentially a typical disruptive technology as it would be very economical and would have exquisite brain source spatial resolution. Similarly to state-of-the-art EEG, DESTIN could become universally present as a non-invasive human brain imaging in any neuroscience center worldwide.

Despite its great success and demonstrated potential for brain imaging, significant limitations exist with EEG, most important of which is the accuracy of the localization of the brain sources from the recorded EEG. This localization is accomplished by using various numerical processing techniques that estimate the set of current sources, which are best approximated by current-dipoles in the brain that best fit the EEG data. The accuracy of the localization processing is affected by a number of factors including: anatomical and electrical (i.e., conductivity) head-modeling errors, source-modeling errors, and noise in the EEG due to the recording instrument or physiology [1-10]. According to Baillet et. al. [11] temporal/spatial accuracy should be at least better than 5mm/5ms. However, in practice this goal is rarely achieved since the mathematical procedure underlying the source localization is ill-posed and the localization problem accepts multiple solutions, which are different sets of sources located in the brain that equivalently predict the EEG measurements. Researchers can only attempt to mitigate the effect of the ill-posedness with numerical strategies and are often required to justify their source localization results with a-priori knowledge about the location of the sources, which may defeat the purpose of source localization.

2. Theory.

The problem of locating large (e.g., patches of cortex of 10 mm² or more) networks of firing neurons inside the brain is similar to the problem of locating low frequency EM sources underwater or in a conductive medium. Low frequency EM methods have been developed as underwater navigation systems due to the fact that standard Global Positioning System (GPS) satellite signals cannot be received at depth. These underwater GPS systems have been employed in scuba diving navigation for such purposes as to seek and destroy unexploded ordinance, underwater crime scene investigation and security inspections, underwater site mapping for fish farms, and marine archeology including artifact mapping and geophysical explorations [12]. Although mostly based on sonar technology, the state-of-the-art underwater GPS systems fuse electromagnetic and acoustic data for increased accuracy and signal-to-noise ratio (SNR). EM-tomography or source localization is based on data recorded from electrodes (i.e., underwater electric field sensors array) [13]. Assuming that a plane wave is generated parallel to the surface of the water, the electromagnetic wave in a dispersive medium is characterized by the following electric and magnetic field

amplitudes: $E(t) = E_0 e^{-i\omega t - d/d_0}$ and $B(t) = B_0 e^{-i\omega t - d/d_0}$, where E_0 and B_0 are the electric and magnetic wave field vector amplitude at the sea surface, ω is the angular frequency of the wave ($f = \omega/2\pi$), $i = \sqrt{-1}$, and d is the depth ($d_0 = 1m$). The wave propagates in vacuum at the speed of light $v = c = 1/\sqrt{\mu_0 \epsilon_0} = 3 \cdot 10^8 m/s$, where: $\mu_0 = 4\pi 10^{-7} Tm/A$, $\epsilon_0 = 1/(36\pi) 10^{-9} F/m$. However, in a dispersive medium such as seawater, the speed is slower and frequency dependent, namely: $v(\omega) = \sqrt{\omega/(2\mu_0 \sigma)}$, where $\sigma \gg \omega \epsilon_0$ is the conductivity (e.g., seawater has conductivity $\sigma \cong 4 S/m$). As the wave propagates in water both its amplitude and phase varies according to the propagation factor: $\gamma(\omega) = \alpha(\omega) + i\beta(\omega)$, where $\alpha(\omega) = \beta(\omega) = \sqrt{\omega \mu_0 \sigma / 2}$ [14]. The power of the wave $A(\omega, d)$ attenuates logarithmically with depth: $A(\omega, d) = \alpha(\omega) \log_{10}(d)$ and at a typical EM-tomography frequency of 25 kHz the power loss is 5.46dB and a phase shift of 0.2π radians (or 36.0°) per meter of seawater depth. A very low frequency (VLF) receiver array data is typically used to receive in each point of the array the amplitude and phase of the signal, which are then used to estimate the source location via the least squares error method.

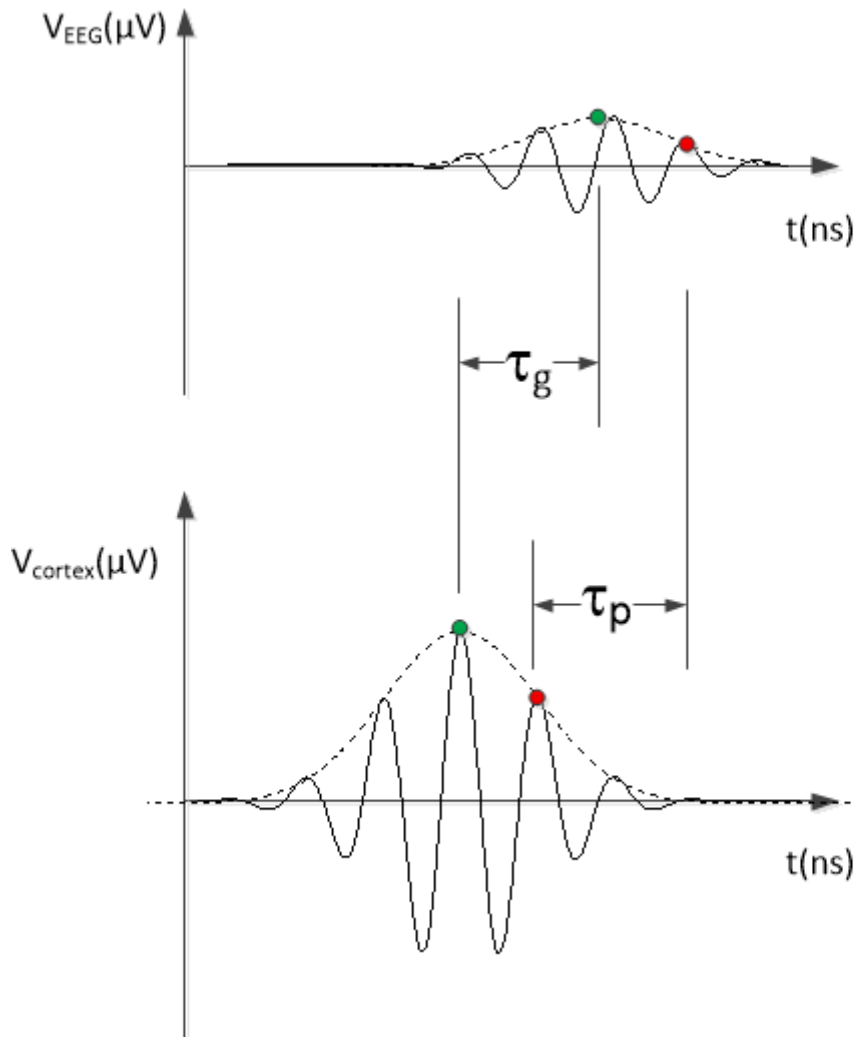


Fig. 1: In the head, the EEG signal propagates from the cortical patch (V_{cortex}) to the EEG electrode (V_{EEG}) at distance d with phase speed $v_p = d/\tau_p$ (in red) and a group speed $v_g = d/\tau_g$ (in green).

Therefore, EM-tomography uses electric field sensor arrays to detect amplitude and phase of electromagnetic waves to estimate the location of the source, knowing only

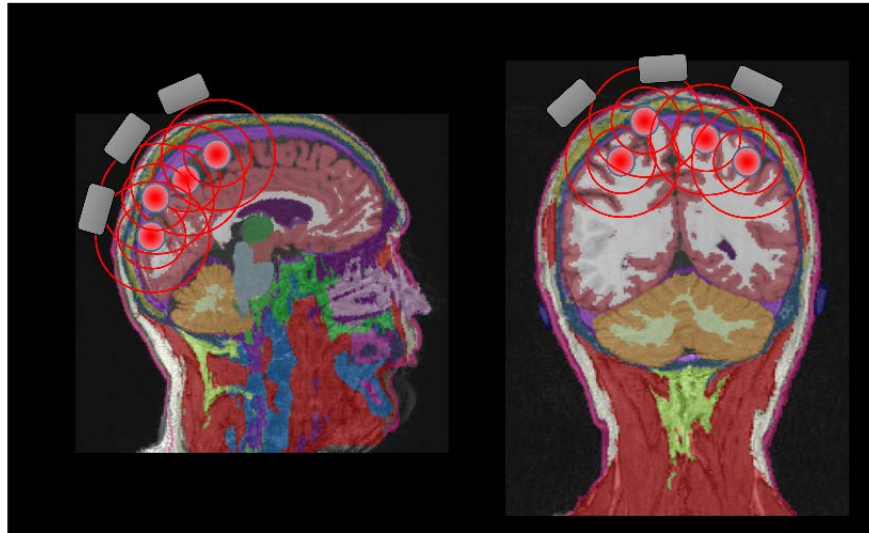
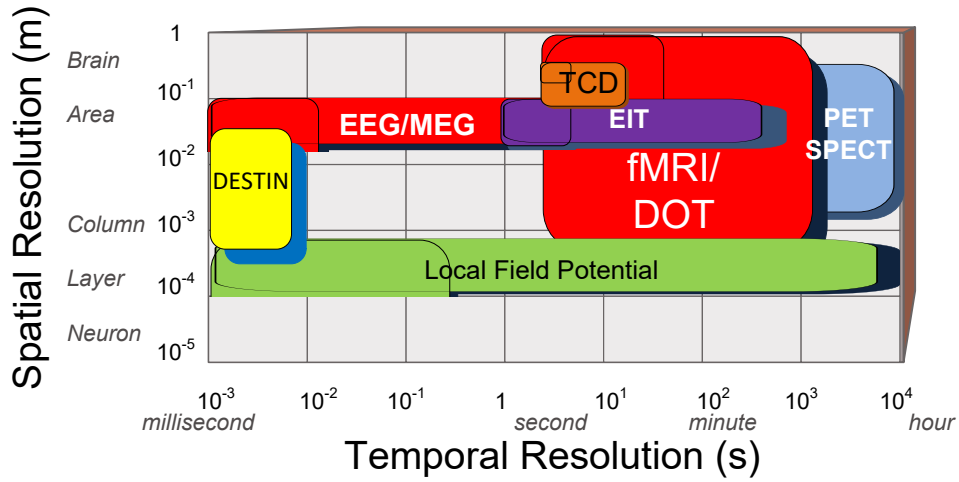


Fig. 2: (Top) Temporal and spatial resolution comparison among different imaging modalities, including: Diffuse Optical Tomography (DOT), EEG, Electrical Impedance Tomography (EIT), functional MRI (fMRI), magnetoencephalography (MEG), Positron Emission Tomography (PET), Single-Photon Emission Computed Tomography (SPECT), Transcranial Doppler (TCD). (Bottom) Sagittal and coronal views of the human head with sources (in red) of neurons firing in cortex and electrodes placed on top of the skull. Depicting the concept of source mixing, in which each electrode “sees” more than one source.

the dispersive properties of the source (i.e., no synchronicity to the source is necessary).

We now describe the propagation in a lossy medium in the case of EEG signals. If we denote with $\sigma(\omega)$, $\mu(\omega)$ and $k(\omega)$ the conductivity, permeability of tissue and the wavenumber, respectively, the group speed is [15]: $v_g = \left(\frac{d k(\omega)}{d \omega} \Big|_{\omega=\omega_0} \right)^{-1}$. The phase speed, or the rate at which the phase of the wave propagates in space, has been studied for low frequency radar propagation in seawater and was estimated as [16]: $v_p = \frac{\omega_0}{k(\omega_0)} = \sqrt{\frac{2\omega_0}{\mu_0\sigma(\omega_0)}}$. In the case of a 10Hz alpha brain-wave ($\omega=20\pi$ rad/s, $\sigma=0.05$ S/m for white matter, $\mu=\mu_0 = 4\pi 10^{-7}$ Tm/A), the phase speed is 44,721 m/s, which is very

close also to the group speed (see below). Just to estimate a ball park delay, if we wish to achieve a 1mm resolution in locating the underlying source and if we assume that no other tissue is present in the path other than white matter, then the propagation delay (**Fig. 1**) is $\tau_p=22.4\text{ns}$. Note that both the phase and the group velocities of EM-waves propagate in empty space at the speed of light ($2.99 \cdot 10^8 \text{ m/s}$), thus more than 6,000× faster through vacuum space than biological tissue. Why is the speed of electromagnetic waves so much slower in tissue? Such a large difference in propagation speed depends on the different mechanism of polarization. At such low frequencies (0-100Hz), the polarization in the tissue is called alpha dielectric dispersion [17], which has been attributed to electronic bilayers in organic molecules, active membrane conductance phenomena, ionic dispersions of micrometer-size particles, etc. [18].

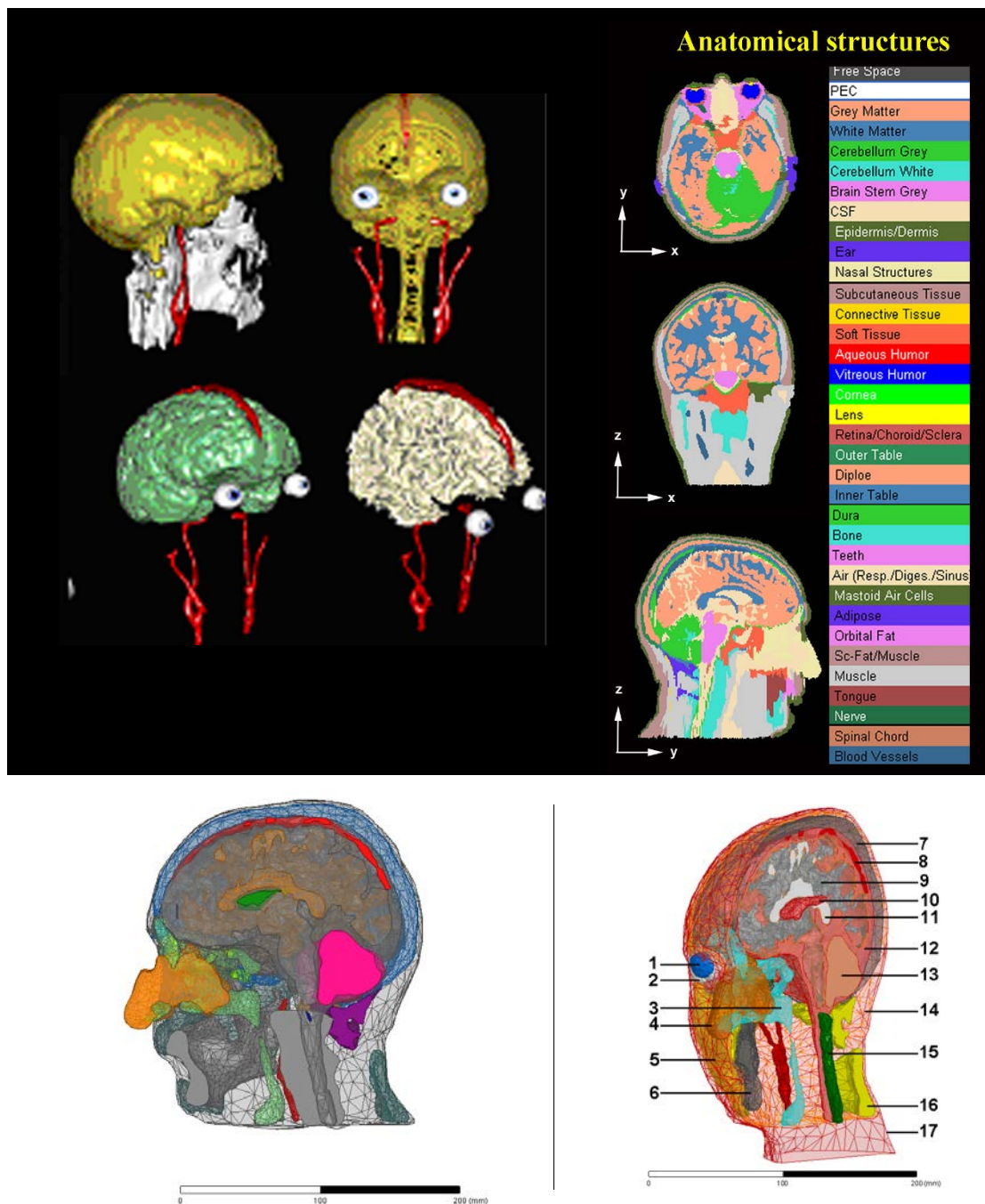


Fig. 3. High-Resolution Head model (1mm^3 isotropic) c.f. the next page

(Top left) 3D views of the internal anatomical structures of the model that allow for realistic anatomical representation [19] ; (Top-right) anatomical structures axial, coronal, and sagittal planes are shown. The corresponding color code for each modeled structure is to the right of the image. (Bottom) The same head model was converted for our FEM simulations [20] (with tissues: 1. retina, 2. orbital fat, 3. sinus, 4. nose, 5. subcutaneous fat, 6. facial bones, 7. skull, 8. blood vessel, 9. grey Matter, 10. CSF, 11. Ventricle, 12. white matter, 13. Brain parenchymal, 14. Cerebellum, 15. Muscle, 16. Spinal cord, 17. Adipose fat, and 18. Skin).

For EM-waves propagation distances in the human head (i.e., $d < 20\text{cm}$), we can assume that the phase and group velocities are approximately the same. The phase of the EM-wave will build up over space according to the phase/group velocities or mathematically: $E(z, t) = E_0 e^{-kz - i\omega_0 t}$, where $k = \alpha - i\beta$ is the complex wave number that depends on ϵ_r [15]. Finally, the relatively low conductivity produces an attenuation of the source signal at the EEG electrode site due to the lossy properties of the dispersive media of the human head.

Studying the wave propagation at low frequency in one dimension, like in the case of seawater, is definitely an oversimplification as the EEG EM-tomography problem is truly three-dimensional. The distribution of the electric field of both amplitude and phase over the scalp surface where the EEG electrodes are located is dependent on dipole: position, orientation and strength. Given the complexity of this problem, it is possible to estimate the wave propagation using only numerical simulation approaches. The idea presented in this paper is rather revolutionary in the EEG field since EEG forward modeling is commonly performed under the static approximation of Maxwell Equations:

$$\begin{aligned}\nabla \times \mathbf{E} &= 0 \\ \nabla \times \mathbf{H} &= \mathbf{J} \\ \nabla \cdot \mathbf{E} &= \frac{\rho}{\epsilon_0} \\ \nabla \cdot \mathbf{H} &= 0\end{aligned}\quad (1)$$

And the group delay is in this case:

$$\tau_g = \lim_{\omega_0 \rightarrow 0} \frac{\Delta z}{v_g} = \lim_{\omega_0 \rightarrow 0} \Delta z \left(\frac{d k(\omega)}{d \omega} \Big|_{\omega=\omega_0} \right) = \Delta z \lim_{\omega_0 \rightarrow 0} \left(\frac{\omega_0}{\sqrt{\frac{2\omega_0}{\mu_0 \sigma(\omega_0)}}} \right) = 0 \quad (2)$$

However, according to Einstein's special relativity it is not possible that EEG waves travel faster than the speed of light, therefore we propose solving Maxwell equations without any approximation and by solving instead the entire set of equations. This can be achieved by using numerical EM-solvers, which was shown to estimate accurate fields at arbitrary frequencies in Debye media [21]. Recently, a 3-D simulation of dispersive half-space problem has been carried out to validate EM simulations using Perfectly Matched Layers (PML) boundary conditions with low-frequency propagating waves [22]. Furthermore, the Finite Element Method (FEM) was used to solve general 3-D problems involving ideal of inhomogeneous and dispersive materials showing that

the accuracy of the FEM method is theoretically guaranteed [23]. The accuracy of numerical EM-simulations of course depends also on the accuracy of the parameters used for the different head model tissues. The set of electromagnetic parameters for very many tissue types can be found in published literature [17, 24, 25] and even in online databases [26]. However, these data are based on a mixture of measurements that were performed on different types of animal species, often in vitro and at room temperature. To make matters even worse, the conductivity of biological tissues is often markedly anisotropic and conductivity may vary 6-7 times more when the current is oriented parallel to the fibers in muscle tissue (one of the tissues in our model, **Fig. 3**) [27]. Last, but not least is the electrode interface with the tissue which constitutes a complex geometry to accurately model. For this reason and because conductivity and permittivity values of different tissues may vary from subject to subject, the electrode contact constitutes a burden for this technology, which will require further investigation.

The residual error in source localization studied with Monte Carlo simulations [28] was shown to be inversely proportional to the number of EEG channels, even when fMRI was used as a statistical prior in the localization algorithm (i.e., fMRI weighting). In clinical studies of epileptic patients using cross-validation with intracranial recording of epileptic spikes, Yamazaki and colleagues [29, 30] concluded that 256-channel dEEG provides more precise detection and source localization for presurgical planning than conventional sparse-array EEG. Similarly, we argue that dense array will improve EM-Tomography. The phase delay of our signals suggest detecting time intervals as small as $\tau_p=22.4\text{ns}$: would a technology based on A/D converter sampling rate of 100 MS/s (89.4 MS/s) be sufficient to estimate time of flight¹ of the EEG and separate sources? In order to answer this question we need to examine closely the speed of the EM-waves in the actual human tissue using parametric analysis.

The Z-parameter of the dipole sources can be used to calculate the phase speed (from now on called propagation speed) through the head-medium. In this case, the head can be considered a transmission line with capacitance and inductance per unit length. Using the Z-Parameter, the unit capacitance can be solved as:

$$\text{Im}(Z_{11}) = \left| \frac{1}{j\omega C_L} \right| \rightarrow C_L = \left| \frac{1}{j \cdot (2\pi 10) \cdot (-1769.4)} \right| = 8.99 \cdot 10^{-6} F \quad (3)$$

Plugging this result in the standard characteristic impedance equation yields the unit inductance per unit length:

$$Z_0 = \sqrt{\frac{L_L}{C_L}} \rightarrow L_L = C_L \cdot Z_0^2 = (8.99 \cdot 10^{-6}) \cdot (50)^2 = 22.5 \cdot 10^{-3} H \quad (4)$$

Using the previous results, using transmission line theory the phase speed per unit length can then be computed as [31]:

¹ Time-of-flight measurements are used for distance measurements: a source sends out a short energy pulse (electromagnetic, optical, sound, etc.) and detector measures the time until the reflected pulse is sensed. In most cases the temporal accuracy must be very high for instance 1 ns resolution is needed for a spatial accuracy of 15 cm in the case of a light pulse travelling in air.

$$v_L = \sqrt{\frac{1}{L_L \cdot C_L}} = \sqrt{\frac{1}{(22.5 \cdot 10^{-3}) \cdot (8.99 \cdot 10^{-6})}} = 2.22 \cdot 10^3 \frac{m}{s} \quad (5)$$

The result is then scaled by the distance between the two sources to compute the phase speed of the system:

$$v = \frac{v_L}{l} = \frac{(2.22 \cdot 10^3)}{(100 \cdot 10^{-3})} = 22.2 \cdot 10^3 \frac{m}{s} \quad (6)$$

This value is reasonably lower than the single tissue value computed analytically on white matter of 44,721 m/s, since electrical properties of other tissues are different from white matter and low frequency scattering [32] occurs. It is important to actually measure this speed, since the simulations predict a speed 15 times the speed of sound in water (i.e., 1,500m/s), which makes many of the sonar techniques very relevant to EEG source localization.

3. Methods.

3.1 Electromagnetic Simulations

Simulations were carried out using the FEM solver ANSYS HFSS 2014 (ANSYS, Canonsburg, PA). An anatomically accurate human head model (**Fig. 3**) was derived from MRI scans [19] containing 22 anatomical structures consisting of 14 unique tissue types. Parameters of the electrical conductivity and dielectric permittivity were taken from [33]. In order to estimate the electric field around two neural generators located deep in the parietal lobe (**Fig. 3, left**) and below the electrode Cz, the head model was augmented with two dipole antennas (i.e., 5mm long \times 5mm diameter) placed tangential to the skull and perpendicular to each other in the grey matter tissue of the brain at a relative distance of 20mm from one another. In order to study the propagation speed between the two antennas, each antenna was driven with a 1W power source with a characteristic impedance of 50 Ω . The model was meshed and solved at a solution frequency of 10Hz, the relevant EEG frequency of interest. The FEM boundary conditions was either perfect matched layer (PML), absorbing boundary conditions (ABC) on Debye media. The accuracy of numerical EM-simulations will of course depend also on the accuracy of the parameters used for the different head model tissues. The set of electromagnetic parameters for very many tissue types can be found in published literature [17, 24-26] and even in online databases [33].

Two dipoles were randomly selected in the gray matter and centered in D1(11mm,0mm,35mm) and D2(-9mm,0mm,30mm) inside the head model (**Fig. 3**). These dipoles were excited with a power of 219pW to produce scalp potentials in the range of tens of μ V similar to EEG signals of healthy subjects. Potentials were estimated in MATLAB on the skin of the model in the following points: Above Dipole 1 (11mm, 0mm, 79.7mm), Above Dipole 2 (-9mm, 0mm, 82.3mm), Above Mastoid or reference point (-47.8mm,71.0mm, -53.5mm), Above Temporal (70mm, -55.8, 15mm), Above Frontal (0mm, -83.8mm, 0mm), Above Occipital (-70mm, -64.0mm, 0mm).

3.2 Independent Component Analysis.

The EEG signal is often considered a very noisy signal - with power spectra diminishing at the $1/f$ rate - and there are indeed a large number of noise sources that may affect the scalp recordings including: environmental (e.g., 50/60Hz line noise, interference from instrumentation or computers, etc.), physiological (e.g. muscle artefact during speaking, head tilting during respiration, electrocardiogram, etc.). However, although these artifacts maybe several times larger than EEG, efforts in quality control and signal processing may lead to an EEG SNR recording of 20dB or better since the EEG instrumentation noise (i.e., amplifier noise, impedance noise and quantization) is usually very small [34]. The challenge in this method consists instead in separating the contributions of the different sources in the brain sensed by each electrode (**Fig. 2, bottom**). One of the most common approaches is blind source separation [35] or independent component analysis (ICA). The ICA problem consists in recovering linearly mixed sources without assuming any a priori knowledge of the original EEG signals besides their statistical independence [36]. Improvements included a two-stage separation process with: a priori selection of an over-complete dictionary based on wavelet frames or learned signals in which the sources are assumed to be sparsely representable, followed by blind decomposition of the sources by exploiting their sparsity [37]. A different approach, the blind decomposition, is a generalized eigenvalue decomposition that simultaneously diagonalizes the covariance matrix of the observations and an additional symmetric matrix whose form depends on the assumptions of non-Gaussian, non-stationary, or non-white independent sources [38].

Since both amplitude A (as a standard EEG) and phase φ are collected, we can consider our DESTIN signals as complex valued: $x(\omega) = A(\omega)e^{j\varphi}$. In this section we introduce a new concept, at least in field of EEG: complex-valued ICA and show numerical examples. The problem consist in finding a linear transformation W , called de-mixing matrix, such that applied to an multichannel signal x produces a multichannel output $y = W^*x$, where W^* is the complex conjugate of W , such that the signals in each channel are maximally statistically independent from each other. When ICA is applied to standard EEG it is used in source localization given its ability to separate brain sources from each other and from external noise (e.g., in EEG/fMRI). In our case, $\overline{x \cdot x^T} + \overline{x \cdot x^*} = \emptyset + i\mathbf{I}$ is the complex autocorrelation of the DESTIN vector which are signals that are zero-mean (i.e., \emptyset) unit variances (i.e., \mathbf{I}) and uncorrelated real and imaginary parts of equal variances. Considering the following cost function:

$$C_F = \sum_{k=1}^N \overline{F(|w_k x|^2)} \quad (7)$$

where the $F()$ is a smooth and non-linear contrast function $F: \mathfrak{R}^+ \cup \square \square \square \rightarrow \mathfrak{R}$, w_k is the k th row of the N -dimensional complex weight W such that $|W^*x| = 1$. Bingham and Hyvärinen have formally proven that the extremes of the cost function C_F in eq.(9) coincide with the independent components [39]. In the DESTIN case, we select the Kurtosis for contrast function [40]:

$$F(r) = \frac{|\overline{r}|^4 - 2|\overline{r}|^2 - |\overline{r^2}|^2}{|\overline{r}|^2} \quad (8)$$

In the following MATLAB example, we show how the proposed algorithm performs in terms of de-mixing a complex noiseless signal. When we select $x = w_{1,1}^r \sin(\omega t) + w_{1,2}^r \cos(\omega t) + w_{2,1}^r \sin(\omega t) + w_{2,2}^r \cos(\omega t) + j * (w_{1,1}^i \sin(\omega t) + w_{1,2}^i \cos(\omega t) + w_{2,1}^i \sin(\omega t) + w_{2,2}^i \cos(\omega t))$, the complex ICA is capable of correctly recovering the two harmonic functions. The proposed algorithm correctly reconstructs the phase of the two mixed signals (i.e., 90°) with a precision of: $\left| \frac{\pi}{2} - \arccos\left(\frac{y_1 y_2}{|y_1| |y_2|}\right) \right| = 1.4211 \cdot 10^{-13}^\circ$, or well within the specifications of this project.

3.3 Time of Flight based Localization.

Let's assume that the brain produces sinusoidal function, since by Fourier series any signal can always be decomposed. The change in signal amplitude for the lowest frequency of interest $\omega_0=1\text{Hz}$, over the desired spatial resolution of $d=1\text{mm}$ and given the speed $v=22,000\text{m/s}$ of EM waves propagation (see above, computed @10Hz at the center of the instrument range of 1-100Hz), is given by:

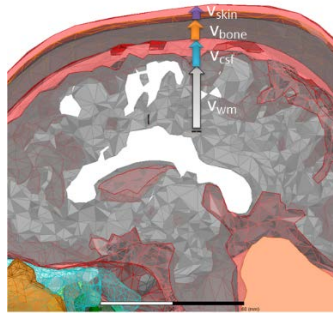
$$\Delta V = \sin(\omega_0 t) - \sin\left(\omega_0\left(t + \frac{d}{v}\right)\right)\Big|_{t=0} = \sin(\omega_0 0) - \sin\left(\omega_0\left(0 + \frac{d}{v}\right)\right) \cong \omega_0 \frac{d}{v} = 2.830\mu V \quad (9)$$

Therefore, if the brain sinusoidal signals had amplitudes of 1V this would require $[-\log_2(2.830 \cdot 10^{-6})]$ or 18 bits. However, since the EEG has amplitudes in the microvolt range, which normally requires at least 12-bits A/D, we would nominally need a minimum of 30 bits to capture such small phase changes instantaneously. An A/D converter with 30 bits and $f_{\text{samp}}=100\text{MS/s}$ rates is well beyond current or foreseeable near-future technology. Thus, phase estimation in time domain (TD) seems to be quite challenging and we recommend instead a frequency domain (FD) design approach instead.

In the human head the speed of the signal will depend on the tissue through which the electromagnetic wave is traveling (**Fig. 4, top**). For simplicity, in the case of a single tissue, the source-sensor delay "τ" [41] is assumed to be equal the difference between the distances of the source (x_s, y_s, z_s) to the corresponding sensor (on the surface of the skin) divided by the speed of the EM-wave v in the tissue. In general, the source position can be found by solving the following set of three quadratic equations:

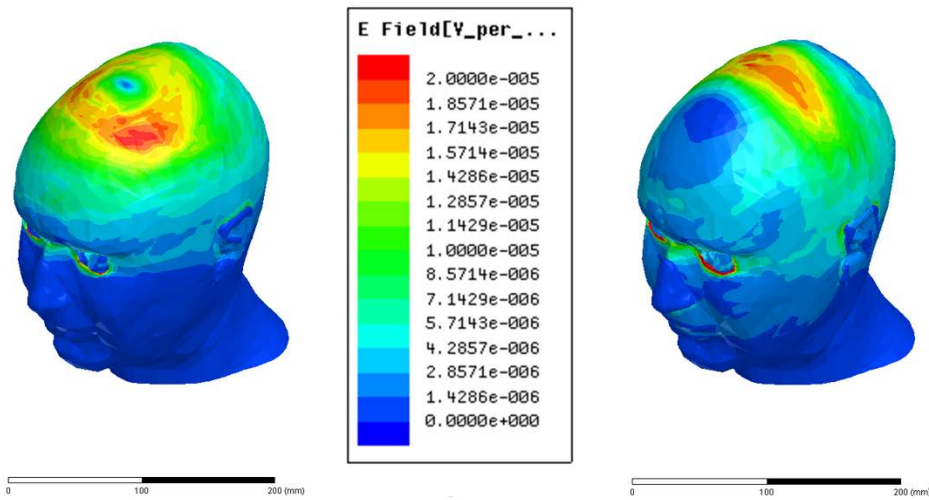
$$\begin{cases} r_o^2 = (x_o - x_s)^2 + (y_o - y_s)^2 + (z_o - z_s)^2 \\ r_f^2 = (x_f - x_s)^2 + (y_f - y_s)^2 + (z_f - z_s)^2 \\ r_t^2 = (x_t - x_s)^2 + (y_t - y_s)^2 + (z_t - z_s)^2 \end{cases} \quad (10)$$

Where $(x_o, y_o, z_o), (x_f, y_f, z_f), (x_t, y_t, z_t)$ are the coordinates of the three sensors, and $r = v_{wm}\tau_{wm} + v_{csf}\tau_{csf} + v_{bone}\tau_{bone} + v_{skin}\tau_{skin}$ is the distance traveled by the EM-wave (e.g., spherical) in the tissue (**Fig. 4 A**).



A.

C.



B.

D.

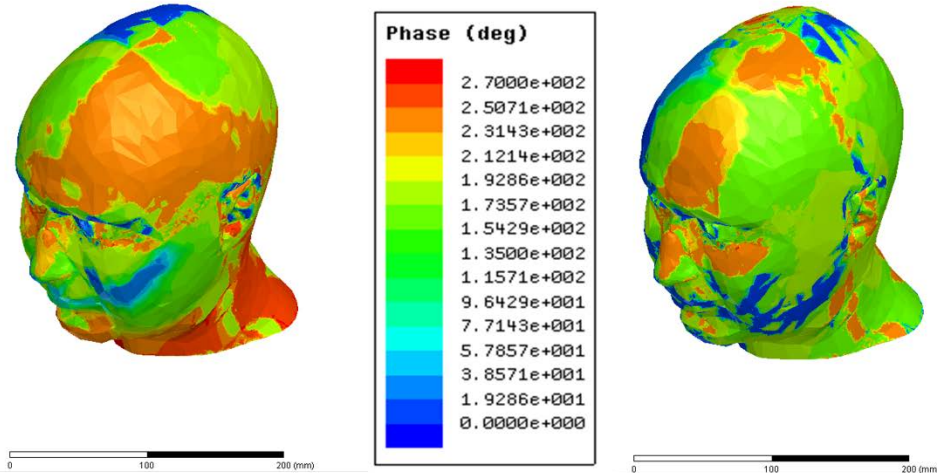


Fig. 4: Example of HFSS phase overestimation at 100Hz in a heterogeneous head. (Top) The dipole E-field wave travels from the dipole to the surface through the Grey/White Matter with velocity v_{wm} , then through CSF, bone and skin. (Bottom) Electric Field (EF) left Source: magnitude (A) and phase (B); EF-right source (C) and (D). The new simulations show that the voltage changes in C_z from $3.774\mu V$ to $2.819\mu V$ or $\approx 1\mu V$ when the horizontal dipole moves 1mm anteriorly-posteriorly, whereas the other dipole generates a $\approx 0.2\mu V$ increase for the same 1mm step starting at $6.05\mu V$.

4. Results.

In order to preliminarily design the nano-radians phase detection technology proposed, we need to precisely characterize the speed of low frequency EM waves to establish the sensitivity required in our measurements. The theoretical phase delay of our signals suggest detecting time intervals as small as $\tau_p=22.4\text{ns}$: would a technology based on A/D converter sampling rate of 100 MS/s (89.4 MS/s) be sufficient to estimate time of flight of the EEG and separate sources? Thus, we performed pilot numerical simulations for an estimate of propagation speed. The iterative FEM solution took approximately 10 hours to solve using a PC with 32 processing cores, required 191GB of RAM, and the maximum change in scattering parameters between subsequent solution passes converged to within 0.5%. The FEM simulations in **Fig. 4** and in **Table 1** show an overestimation of the predicted phase changes of the signal over the skull surface, since HFSS is operating beyond its frequency range (i.e., $< 200\text{kHz}$).

Again, eq.(8) is solved numerically with a proof-of-principle example (neglecting the effect of noise and scattering) to illustrate the localization more clearly by fixing the (x,y,z) position of the three DESTIN sensors for example to: (f) frontal (70,-55.8,15) (mm), (t) temporal (0,-55.8,0) (mm), and (o) occipital (-70,-4.0,0) (mm). If the source is located in: S (1, 0,35) (mm) and $v_{wm} = \sqrt{\frac{200\pi}{0.0894\pi 10^{-7}}} = 74,953 \text{ m/s}$, and $v_{csf} = \sqrt{\frac{200\pi}{2.4\pi 10^{-7}}} = 15,811 \text{ m/s}$. Depending where F, T and O are located we can estimate the thickness, thus eliminating extraneous variables. From our numerical head model: $r_f = v_{wm}\tau_{wm}^f + (2.33 + 5.83 + 2.12)\text{mm}$, $r_t = v_{wm}\tau_{wm}^t + (2.88 + 4.04 + 2.38)\text{mm}$ and $r_o = v_{wm}\tau_{wm}^o + (3.92 + 7.2 + 2.87)\text{mm}$. We can estimate $\tau_{wm}^f = \tau_F - \tau_{csf}^f - \tau_{bone}^f - \tau_{skin}^f$, using again velocity from conductivity and thickness from the model as done above we estimated the following propagation delays: $\tau_{wm}^o = 1.64 \mu\text{s}$, $\tau_{wm}^t = 1.2853\mu\text{s}$, $\tau_{wm}^f = 2.1252\mu\text{s}$. Using MATLAB (x=fsolve(@(x) tdoa(S,Po,Pf,Pt,r),zero)) the solution (11,0,35) of eq.(11) was found (the closed form analytical solution exists and it is quite simple!) with an error less than 1 μm ($-2.2 \cdot 10^{-8}$, $1.9 \cdot 10^{-7}$, $1.0 \cdot 10^{-7}$) (m) and in a fraction of a second (i.e., 47ms) running on a laptop in Windows 8.1.

5. Discussion.

Direct Electromagnetic Source Tomography Imaging Neurotechnology (DESTIN), is a new type of EEG system specifically designed for the localization of EEG current sources in the brain. Unlike the indirect and sluggish hemodynamic response measured by fMRI [42-49], DESTIN has the potential to provide a direct measure of neuronal activity with the exquisite millimeter/millisecond resolution of EEG. Importantly, however, direct tomography would overcome the main limitation of EEG, namely, poor and error-prone estimation of brain sources from scalp recordings due to the inherent ill-posed nature of the inverse method.

In order to build a first DESTIN prototype, a set of design specifications are necessary for a correct lock-in amplifier (LIA) for phase estimation. The LIA for accurate phase detection (**Fig. 5**) has already been successfully employed in steady-state evoked potential delay estimation in EEG [50].

<i>Source 1 ON</i>	<i>Above Dipole 1</i>	<i>Above Dipole 2</i>	<i>Above Frontal Lobe</i>	<i>Above Temporal Lobe</i>	<i>Above Occipital Lobe</i>
-1mm	7.9μV	3.8μV	2.7μV	0.9μV	0.6μV
0mm	6.5μV	2.8μV	2.7μV	0.8μV	0.6μV
+1mm	6.1μV	2.9μV	2.8μV	0.8μV	0.6μV
-1mm	260°	179°	113°	195°	101°
0mm	218°	170°	18°	179°	88°
+1mm	294°	176°	109°	251°	61°

<i>Source 2 ON</i>	<i>Above Dipole 1</i>	<i>Above Dipole 2</i>	<i>Above Frontal Lobe</i>	<i>Above Temporal Lobe</i>	<i>Above Occipital Lobe</i>
-1mm	7.4μV	6.1μV	1.9μV	1.1μV	0.6μV
0mm	7.6μV	6.2μV	2.0μV	1.1μV	0.6μV
+1mm	10.1μV	8.2μV	2.5μV	1.6μV	0.8μV
-1mm	250°	127°	177°	13°	308°
0mm	231°	171°	176°	15°	243°
+1mm	200°	109°	164°	60°	256°

Table 1: Example of phase over estimation with HFSS. Scalp potentials (top rows) and phases (bottom) estimated with HFSS when moving two sources $\pm 1\text{mm}$. The two sources are two dipoles centered in $D1(11\text{mm}, 0\text{mm}, 35\text{mm})$ and $D2(-9\text{mm}, 0\text{mm}, 30\text{mm})$.

LIA is based on simple harmonic analysis: if $V(t) = V_0 \sin(\omega_0 t + \varphi)$ is the input signal and if the heterodyne potential is $V_H(t) = V_H \sin(\omega_H t + \beta)$, the product gives harmonic components (i.e., beats) at the sum and difference frequencies, and when the input and the heterodynic signals are the same:

$$\frac{V_0 V_H}{2} [\cos((\omega_0 - \omega_H)t + \varphi + \beta) - \cos((\omega_0 + \omega_H)t + \varphi + \beta)]_{\omega_0 = \omega_H, \beta = 0} = \frac{V_0 V_H}{2} [\cos(\varphi) - \cos(2\omega_0 t + \varphi)] \quad (11)$$

If we measure the DC component by filtering out the high-frequency part in eq. (6), leading to the estimation of φ numerically. The high frequency filtering will discard any residual noise and any instrument/environment noise component at ω_0 frequency will also be rejected. How many bits do we really need? The total number of bits needed for a digital LIA is given by the more realistic estimate [51]:

$$b = \left\lceil 1.33 + \log_2 \left(1 + \frac{1}{\tan(\varphi_{min})} \right) \right\rceil \quad (12)$$

Given that $\varphi_{min} = \min_{1 \leq f \leq 100} 2f\pi \frac{d}{r \cdot v(f)} = 172.4 \text{ nrad}$ (considering that $v(1\text{Hz}) \approx 3,644 \text{ m/s}$, $v(10\text{Hz}) = 22,200 \text{ m/s}$ and $v(100\text{Hz}) = 32,923 \text{ m/s}$ and $r = 10$ (i.e., an error below $5 \times$ Nyquist phase sampling rate that corresponds to nano-radians resolution) which is feasible to detect [52] and corresponds to $b = 24$ bits at an EEG sampling rate of 1 kS/s , this type of A/D converter technology with a highly synchronous module is

readily available (e.g., $b=31$ and $fsamp=4kS/s$, ADS1281, Texas Instruments, Dallas TX). The signal from each EEG channel after A/D can be numerically filtered with analog narrow pass-band filters or FFT at various harmonics (e.g., 10, 20, .., 80) and fed to the multifrequency digital LIA for phase detection after measuring each of the various harmonic amplitudes. Given the large channel by channel variances in the human recordings of trans-impedances and the accuracy of our numerical head models, we expect that the high density (HD) array of sensors proposed (i.e., 256) will be needed for similar reasons to dEEG. Finally, passive source localization based on time difference of arrivals (TDOAs) [53-55] has been thoroughly tested in the presence of multiple sources [56, 57].

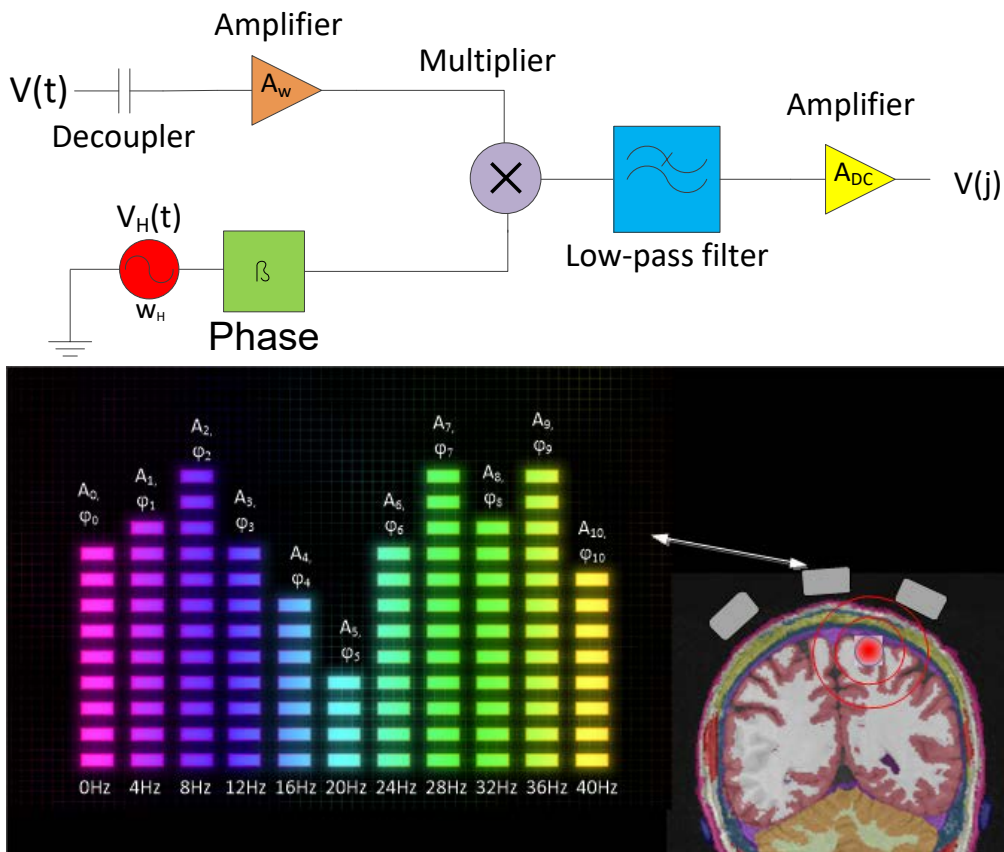


Fig. 5: The proposed lock-in amplifier (LIA). (Top) General schematics of the circuit. (Bottom) An example of spectrogram of an in terms of amplitude and phase (left) and the coronal view of a human head with a source (red) representing the area where neurons are firing and on top the electrodes, which depicts that LIA will allow for channel by channel precise spectral phase estimation.

A potential system made of the 256 channels is shown in **Fig. 6**, which accommodates amplitude and phase estimation at DC and at a set of 10 different frequencies $\Gamma \in \{0Hz, 4Hz, \dots, 40Hz\}$. Furthermore, each channel may include a complex impedance measurement system at Γ . The computer, is connected via an

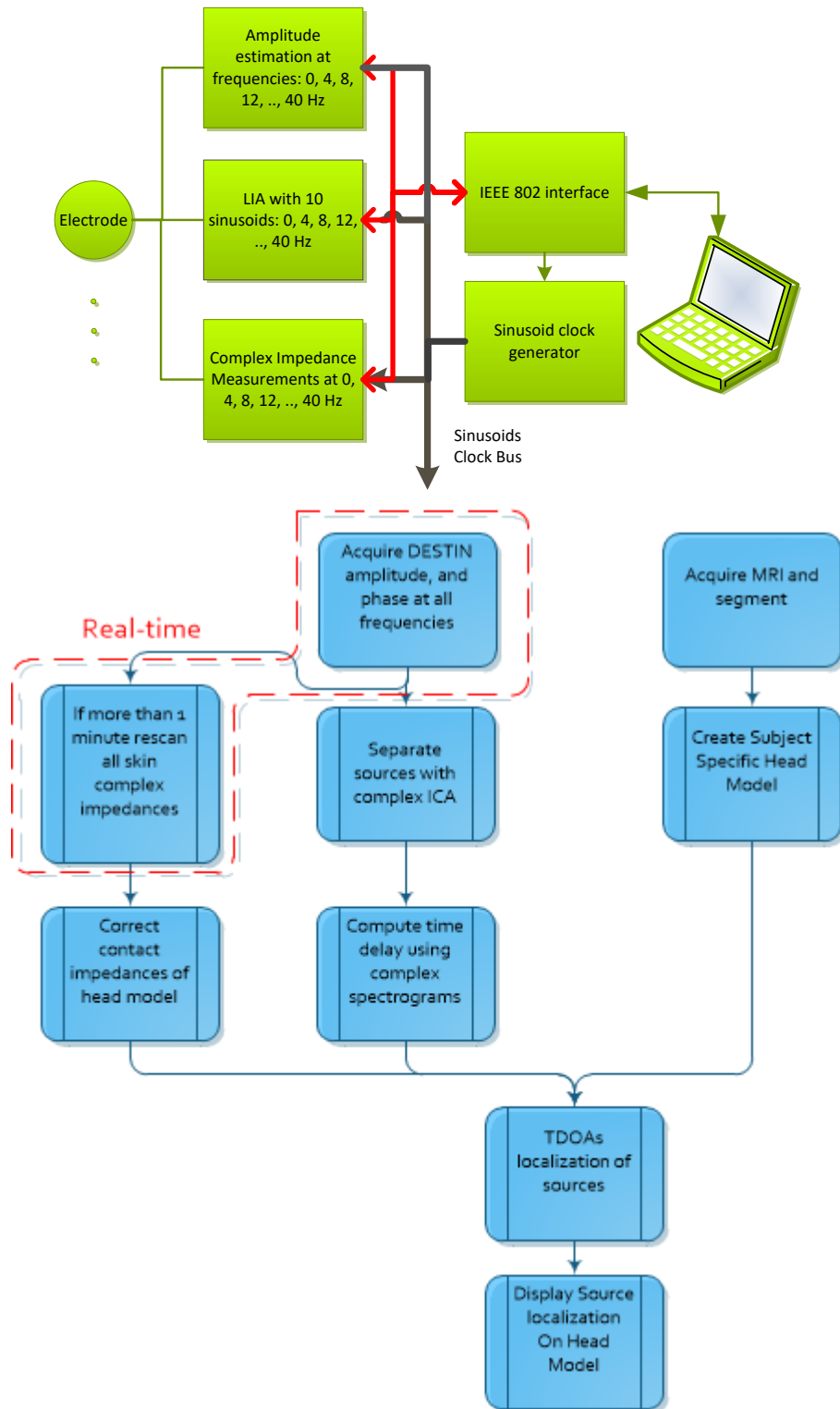


Fig. 6: Architecture of DESTIN. (Top) HW layout. (Bottom) SW Flowchart. In this figure we used the following abbreviations: IEEE 802 stands for Ethernet and Wi-Fi, ICA is independent component analysis, TDOA is the Time Difference of Arrival

internet interface to DESTIN, via a controller that will supervise power and the sinusoidal bus controller (**Fig. 6 Top**). The software architecture consists of modules for controlling the instrument for real time spectral and complex impedance estimation. Off line, the software should allow for automatic model segmentation, separate sources,

estimate source localization and display sources overlaid onto the subject specific head model.

The EM modeling used for propagation of the signal in the tissue employed the transmission line to model the human head. This type of approximation has been introduced previously for a very large spectrum of frequencies and disparate bio-electromagnetic problems [27, 58-62] with very high precision. The assumptions made when using a transmission line and the consequent limitation is due to the assumption of *linearity*, or in other words the circuit or quadrupole can be modeled as a RLC circuit. However, such circuit has dispersive component or the circuit is made of $R(\omega)$, $L(\omega)$ and $C(\omega)$ and in this case the RLC circuit models can model the tissue very precisely (e.g., the Cole–Fricke–Cole model [63]). Using such RLC model, electrical impedance spectroscopy (EIS) at low frequency reveals parameters that are dominated by the motility of the ions that carry the electric field [18], confirms that the actual speed v of low frequency electromagnetic waves in tissue is approximately the speed of sound in water.

Finally, limitations include that the electrode interface with the tissue constitutes a complex geometry to accurately model. For this reason and because conductivity and permittivity values of different tissues may vary from subject to subject, accurate numerical head modeling is limited by the accuracy of such values.

The testing of this system could be performed to study phase distributions by injecting very small current into a patient’s scalp and recording the phases ([64] and [65]). Retinotopic eccentricity [66, 67], could help assess DESTIN localization accuracy signal of the visual evoked potential (VEP) experiment, in which a flashing object is displayed in a precise location in the subject’s visual field which projects into visual cortex through the retinotopic mapping. DESTIN localizations could be compared to the retinotopic predictions. MRI of healthy subjects maybe required for accurate head modeling to develop a system that is robust and subject-specific. Testing in humans could elucidate whether the gain difference of arrivals (GDOA) information (known to improve localization [68]), and phase difference of arrivals (PDOA) information works best (see below). Although, all new methods must be tested against Crammer-Rao bound localization limits [69]. The delay estimation algorithm is the most important component of the entire DESTIN system, and its accuracy will decide the final spatial resolution of the entire instrument. The delay (or phase) computation relies on the similarity of the signal as it is picked up by the different sensors. Detailed validation should be performed on individual head modeling to study the accuracy of the simulations against the EIS recordings performed on all subjects.

6. Conclusions.

Direct tracking would overcome the main limitation of EEG, namely, poor and error-prone estimation of brain sources from scalp recordings due to the inherent ill-posed nature of the inverse method. This new approach may displace the currently outdated EEG technology providing a direct measure of neuronal activity with the exquisite millimeter/millisecond resolution of EEG at low cost and high degree of portability for real world measurements.

In this manuscript we have presented how DESTIN could potentially be implemented with respect to localization, including accurate phase estimation with the use of a proposed lock in amplifier (LIA). The localization is entirely based on the theory that predicts that EM-waves propagate much slowly in the brain than in vacuum

(i.e., speed of light), and only about an order of magnitude more than sound in water making direct localization feasible. However, we tested EM-simulation software i.e., HFSS) and found that it greatly overestimates the phases of the signal. Thus a better low frequency phase estimation systems are needed to best study the low frequency EM-wave propagation in the brain. Finally, this paper discusses a possible architecture for HW and SW implementation of DESTIN, using ICA for source separation for the case of multiple sources active at the same time.

7. Acknowledgements.

This work has been partially supported by the NIH grants P41EB015896 and R21EB016449. The author would like to thank Peter Serano from the Food and Drug Administration for the help in preparing some of the figures and FEM simulations.

8. References.

- [1] Babiloni, C., Vecchio, F., Miriello, M., Romani, G. L., and Rossini, P. M., 2006, "Visuo-spatial consciousness and parieto-occipital areas: a high-resolution EEG study," *Cereb Cortex*, 16(1), pp. 37-46.
- [2] Babiloni, F., Babiloni, C., Carducci, F., Fattorini, L., Anello, C., Onorati, P., and Urbano, A., 1997, "High resolution EEG: a new model-dependent spatial deblurring method using a realistically-shaped MR-constructed subject's head model," *Electroencephalography and clinical neurophysiology*, 102(2), pp. 69-80.
- [3] Boughariou, J., Jallouli, N., Zouch, W., Ben Slima, M., and Ben Hamida, A., 2015, "Spatial Resolution Improvement of EEG Source Reconstruction Using swLORETA," *IEEE transactions on nanobioscience*, 14(7), pp. 734-739.
- [4] Gevins, A., Le, J., Martin, N. K., Brickett, P., Desmond, J., and Reutter, B., 1994, "High resolution EEG: 124-channel recording, spatial deblurring and MRI integration methods," *Electroencephalography and clinical neurophysiology*, 90(5), pp. 337-358.
- [5] Im, C. H., Gururajan, A., Zhang, N., Chen, W., and He, B., 2007, "Spatial resolution of EEG cortical source imaging revealed by localization of retinotopic organization in human primary visual cortex," *Journal of neuroscience methods*, 161(1), pp. 142-154.
- [6] Law, S. K., Rohrbaugh, J. W., Adams, C. M., and Eckardt, M. J., 1993, "Improving spatial and temporal resolution in evoked EEG responses using surface Laplacians," *Electroencephalography and clinical neurophysiology*, 88(4), pp. 309-322.
- [7] Nunez, P. L., and Pilgreen, K. L., 1991, "The spline-Laplacian in clinical neurophysiology: a method to improve EEG spatial resolution," *Journal of clinical neurophysiology : official publication of the American Electroencephalographic Society*, 8(4), pp. 397-413.
- [8] Pascual-Marqui, R. D., and Biscay-Lirio, R., 1993, "Spatial resolution of neuronal generators based on EEG and MEG measurements," *Int J Neurosci*, 68(1-2), pp. 93-105.
- [9] Ryyanen, O., Hyttinen, J., and Malmivuo, J., 2004, "Study on the spatial resolution of EEG--effect of electrode density and measurement noise," *Conf Proc IEEE Eng Med Biol Soc*, 6, pp. 4409-4412.
- [10] Yuan, H., Ding, L., Zhu, M., Zotev, V., Phillips, R., and Bodurka, J., 2015, "Reconstructing Large-Scale Brain Resting-State Networks from High-Resolution EEG: Spatial and Temporal Comparisons with fMRI," *Brain connectivity*.
- [11] Baillet, S., Garnero, L., Marin, G., and Hugonin, J. P., 1999, "Combined MEG and EEG source imaging by minimization of mutual information," *IEEE Trans Biomed Eng*, 46(5), pp. 522-534.
- [12] Tossman, B., Thayer, D., and Swartz, W., 1979, "An underwater towed electromagnetic source for geophysical exploration," *Oceanic Engineering, IEEE Journal of*, 4(3), pp. 84-89.

- [13] Persson, L., Dalberg, E., Lauberts, A., and Lennartsson, R. K., 2007, "Performance evaluation of underwater target tracking using data fusion on acoustic and electromagnetic data," *Information Fusion*, 2007 10th International Conference on, pp. 1-7.
- [14] Kullstam, P., 1990, "Underwater carrier phase tracking perturbed by ocean waves," *Military Communications Conference, 1990. MILCOM '90, Conference Record, A New Era. 1990 IEEE*, pp. 1080-1084 vol.1083.
- [15] Orfanidis, J., 2013, *Electromagnetic Waves and Antennas*.
- [16] King, R. W. P., and Wu, T. T., 1993, "The propagation of a radar pulse in sea water," *Journal of Applied Physics*, 73(4), pp. 1581-1590.
- [17] Gabriel, C., Gabriel, S., and Corthout, E., 1996, "The dielectric properties of biological tissues: I. Literature survey," *Phys. Med. Biol.*, 41, pp. 2231-2249.
- [18] Barsoukov, E., and Macdonald, J. R., 2005, *Impedance spectroscopy : theory, experiment, and applications*, Wiley-Interscience, Hoboken, N.J.
- [19] Makris, N., Angelone, L., Tulloch, S., Sorg, S., Kaiser, J., Kennedy, D., and Bonmassar, G., 2008, "MRI-based anatomical model of the human head for specific absorption rate mapping," *Med Biol Eng Comput*, 46(12), pp. 1239-1251.
- [20] Serano, P., Angelone, L. M., Katnani, H., Eskandar, E., and Bonmassar, G., 2015, "A novel brain stimulation technology provides compatibility with MRI," *Scientific reports*, 5, p. 9805.
- [21] Sandeep, S., and Gasiewski, A., 2013, "Transient Analysis of Dispersive, Periodic Structures for Oblique Plane Wave Incidence Using Laguerre Marching-on-in-Degree (MoD)," *Antennas and Propagation, IEEE Transactions on*, 61(8), pp. 4132-4138.
- [22] Naixing, F., and Jianxiong, L., 2012, "Efficient DSP-Higher-Order PML Formulations for the Metal Plate Buried in Dispersive Soil Half-Space Problem," *Electromagnetic Compatibility, IEEE Transactions on*, 54(5), pp. 1178-1181.
- [23] Jianfang, Z., and Dan, J., 2012, "A fast and accurate O(1) solution to the low-frequency breakdown problem of fullwave solvers," *Electromagnetic Compatibility (EMC), 2012 IEEE International Symposium on*, pp. 189-192.
- [24] Gabriel, C., Gabriel, S., and Corthout, E., 1996, "The dielectric properties of biological tissues: II. Measurements in the frequency range 10 Hz to 20 GHz," *Phys. Med. Biol.*, 41, pp. 2251-2269.
- [25] Gabriel, C., Gabriel, S., and Corthout, E., 1996, "The dielectric properties of biological tissues: III. Parametric models for the dielectric spectrum of tissues," *Phys. Med. Biol.*, 41, pp. 2271-2293.
- [26] Gabriel, C., and Gabriel, S., 1996, "Compilation of the dielectric properties of body tissues at RF and microwave frequencies," <http://niremf.ifac.cnr.it/docs/DIELECTRIC/Report.html>.
- [27] Reilly, J. P., 1998, *Applied Bioelectricity : From Electrical Stimulation to Electropathology*, Springer Verlag.
- [28] Liu, A. K., Dale, A. M., and Belliveau, J. W., 2002, "Monte Carlo simulation studies of EEG and MEG localization accuracy," *Hum Brain Mapp*, 16(1), pp. 47-62.
- [29] Yamazaki, M., Terrill, M., Fujimoto, A., Yamamoto, T., and Tucker, D. M., 2012, "Integrating dense array EEG in the presurgical evaluation of temporal lobe epilepsy," *ISRN neurology*, 2012, p. 924081.
- [30] Yamazaki, M., Tucker, D. M., Terrill, M., Fujimoto, A., and Yamamoto, T., 2013, "Dense array EEG source estimation in neocortical epilepsy," *Frontiers in neurology*, 4, p. 42.
- [31] Wadell, B. C., 1991, *Transmission line design handbook*, Artech House, Boston.
- [32] Dassios, G., *Ellipsoidal harmonics : theory and applications*.
- [33] CNR, I., 2016, "Dielectric Properties of Body Tissues in the frequency range 10 Hz - 100 GHz," <http://niremf.ifac.cnr.it/tissprop/>.
- [34] Schlögl, A., Slater, M., and Pfurtscheller, G., 2002, "Presence research and EEG."
- [35] Jutten, C., and Herault, J., 1991, "Blind separation of sources, part I: An adaptive algorithm based on neuromimetic architecture," *Signal Processing*, 24(1), pp. 1-10.

- [36] Delorme, A., and Makeig, S., 2004, "EEGLAB: an open source toolbox for analysis of single-trial EEG dynamics including independent component analysis," *Journal of neuroscience methods*, 134(1), pp. 9-21.
- [37] Zibulevsky, M., and Pearlmutter, B. A., 2001, "Blind source separation by sparse decomposition in a signal dictionary," *Neural computation*, 13(4), pp. 863-882.
- [38] Parra, L., and Sajda, P., 2003, "Blind source separation via generalized eigenvalue decomposition," *J. Mach. Learn. Res.*, 4, pp. 1261-1269.
- [39] Bingham, E., and Hyvarinen, A., 2000, "A fast fixed-point algorithm for independent component analysis of complex valued signals," *International journal of neural systems*, 10(1), pp. 1-8.
- [40] Zarzoso, V., and Comon, P., 2010, "Robust independent component analysis by iterative maximization of the kurtosis contrast with algebraic optimal step size," *IEEE transactions on neural networks / a publication of the IEEE Neural Networks Council*, 21(2), pp. 248-261.
- [41] Gezici, S., Zhi, T., Giannakis, G. B., Kobayashi, H., Molisch, A. F., Poor, H. V., and Sahinoglu, Z., 2005, "Localization via ultra-wideband radios: a look at positioning aspects for future sensor networks," *Signal Processing Magazine, IEEE*, 22(4), pp. 70-84.
- [42] Belliveau, J. W., Kennedy, D. N., Jr., McKinstry, R. C., Buchbinder, B. R., Weisskoff, R. M., Cohen, M. S., Vevea, J. M., Brady, T. J., and Rosen, B. R., 1991, "Functional mapping of the human visual cortex by magnetic resonance imaging," *Science*, 254(5032), pp. 716-719.
- [43] Mantini, D., Marzetti, L., Corbetta, M., Romani, G. L., and Del Gratta, C., 2010, "Multimodal integration of fMRI and EEG data for high spatial and temporal resolution analysis of brain networks," *Brain topography*, 23(2), pp. 150-158.
- [44] Yuste, R., and Fairhall, A. L., 2015, "Temporal dynamics in fMRI resting-state activity," *Proc Natl Acad Sci U S A*, 112(17), pp. 5263-5264.
- [45] He, L., Hu, D., Wan, M., and Wen, Y., 2014, "Measuring temporal dynamics of resting-state fMRI data," *Bio-medical materials and engineering*, 24(1), pp. 939-945.
- [46] Olsen, A., Ferenc Brunner, J., Evensen, K. A., Garzon, B., Landro, N. I., and Haberg, A. K., 2013, "The functional topography and temporal dynamics of overlapping and distinct brain activations for adaptive task control and stable task-set maintenance during performance of an fMRI-adapted clinical continuous performance test," *Journal of cognitive neuroscience*, 25(6), pp. 903-919.
- [47] Hanson, S. J., Gagliardi, A. D., and Hanson, C., 2009, "Solving the brain synchrony eigenvalue problem: conservation of temporal dynamics (fMRI) over subjects doing the same task," *J Comput Neurosci*, 27(1), pp. 103-114.
- [48] Shen, Q., Ren, H., and Duong, T. Q., 2008, "CBF, BOLD, CBV, and CMRO(2) fMRI signal temporal dynamics at 500-msec resolution," *Journal of magnetic resonance imaging : JMRI*, 27(3), pp. 599-606.
- [49] de Zwart, J. A., Silva, A. C., van Gelderen, P., Kellman, P., Fukunaga, M., Chu, R., Koretsky, A. P., Frank, J. A., and Duyn, J. H., 2005, "Temporal dynamics of the BOLD fMRI impulse response," *Neuroimage*, 24(3), pp. 667-677.
- [50] Tamiya, K., Higashidate, M., and Kikkawa, S., 1986, "Technique with lock-in amplifier for real-time measurement of tricuspid valve annulus area," *The American journal of physiology*, 251(2 Pt 2), pp. H236-241.
- [51] Vandenbussche, J. J., Lee, P., and Peuteman, J., 2014, "On the Accuracy of Digital Phase Sensitive Detectors Implemented in FPGA Technology," *Instrumentation and Measurement, IEEE Transactions on*, PP(99), pp. 1-1.
- [52] Dassios, G., and Kleinman, R., 2000, *Low frequency scattering*, Clarendon Press ; Oxford University Press, Oxford (England).
- [53] Barbieri, C. L., Brown, K., and Rabinovitch, M., 1985, "Depletion of secondary lysosomes in mouse macrophages infected with *Leishmania mexicana amazonensis*: a cytochemical study," *Zeitschrift fur Parasitenkunde*, 71(2), pp. 159-168.
- [54] Chan, Y. T., and Ho, K. C., 1994, "A simple and efficient estimator for hyperbolic location," *Signal Processing, IEEE Transactions on*, 42(8), pp. 1905-1915.

- [55] Carter, G. C., 1993, *Coherence and time delay estimation : an applied tutorial for research, development, test, and evaluation engineers*, IEEE Press, Piscataway, NJ.
- [56] Ho, K. C., and Ming, S., 2008, "Passive Source Localization Using Time Differences of Arrival and Gain Ratios of Arrival," *Signal Processing, IEEE Transactions on*, 56(2), pp. 464-477.
- [57] Yegnanarayana, B., Prasanna, S., Duraiswami, R., and Zotkin, D., 2005, "Processing of reverberant speech for time-delay estimation," *Speech and Audio Processing, IEEE Transactions on*, 13(6), pp. 1110-1118.
- [58] Huang, Y., and Dilworth, I. J., 1995, "Three dimensional modelling of EM fields in the human head," *Antennas and Propagation, 1995., Ninth International Conference on (Conf. Publ. No. 407)*, pp. 223-226 vol.221.
- [59] Taflove, A., and Hagness, S. C., 2000, *Computational electrodynamics : the finite-difference time-domain method*, Artech House, Boston.
- [60] Razansky, D., Soldea, D. F., and Einziger, P. D., 2005, "Generalized transmission-line model for estimation of cellular handset power absorption in biological tissues," *Electromagnetic Compatibility, IEEE Transactions on*, 47(1), pp. 61-67.
- [61] John, L. R., "Forward electrical transmission line model of the human arterial system," *Med. Biol. Eng. Comput.*, 42(3), pp. 312-321.
- [62] Dawson, T. W., Caputa, K., and Stuchly, M. A., 1998, "High-resolution organ dosimetry for human exposure to low-frequency electric fields," *Power Delivery, IEEE Transactions on*, 13(2), pp. 366-373.
- [63] Lafargue, A. L., Cabrales, L. B., and Larramendi, R. M., 2002, "Bioelectrical parameters of the whole human body obtained through bioelectrical impedance analysis," *Bioelectromagnetics*, 23(6), pp. 450-454.
- [64] Bonmassar, G., Iwaki, S., Goldmakher, G., Angelone, L. M., Belliveau, J. W., and Lev, M. H., 2010, "On the Measurement of Electrical Impedance Spectroscopy (EIS) of the Human Head," *International journal of bioelectromagnetism*, 12(1), pp. 32-46.
- [65] Salman, A., Turovets, S., Malony, A., Poolman, P., Davey, C., Eriksen, K., and Tucker, D., 2006, "Noninvasive conductivity extraction for high-resolution EEG source localization.," *Advances in Clinical Neuroscience and Rehabilitation*, pp. 27-28.
- [66] Bonmassar, G., Hadjikhani, N., Ives, J. R., Hinton, D., and Belliveau, J. W., 2001, "Influence of EEG electrodes on simultaneous EEG/fMRI measurements.," *Human Brain Mapping*, 14(2), pp. 108-115.
- [67] Sereno, M. I., Dale, A. M., Reppas, J. B., Kwong, K. K., Belliveau, J. W., Brady, T. J., Rosen, B. R., and Tootell, R. B., 1995, "Borders of multiple visual areas in humans revealed by functional magnetic resonance imaging," *Science*, 268(5212), pp. 889-893.
- [68] Yung-Dar, H., and Barkat, M., 1991, "Near-field multiple source localization by passive sensor array," *Antennas and Propagation, IEEE Transactions on*, 39(7), pp. 968-975.
- [69] D'Andrea, A. N., Mengali, U., and Reggiannini, R., 1994, "The modified Cramer-Rao bound and its application to synchronization problems," *Communications, IEEE Transactions on*, 42(234), pp. 1391-1399.